eLIFE elifesciences.org

RESEARCH ARTICLE

Figures and figure supplements

An orphan cbb_3-type cytochrome oxidase subunit supports *Pseudomonas aeruginosa* biofilm growth and virulence

Jeanyoung Jo *et al*

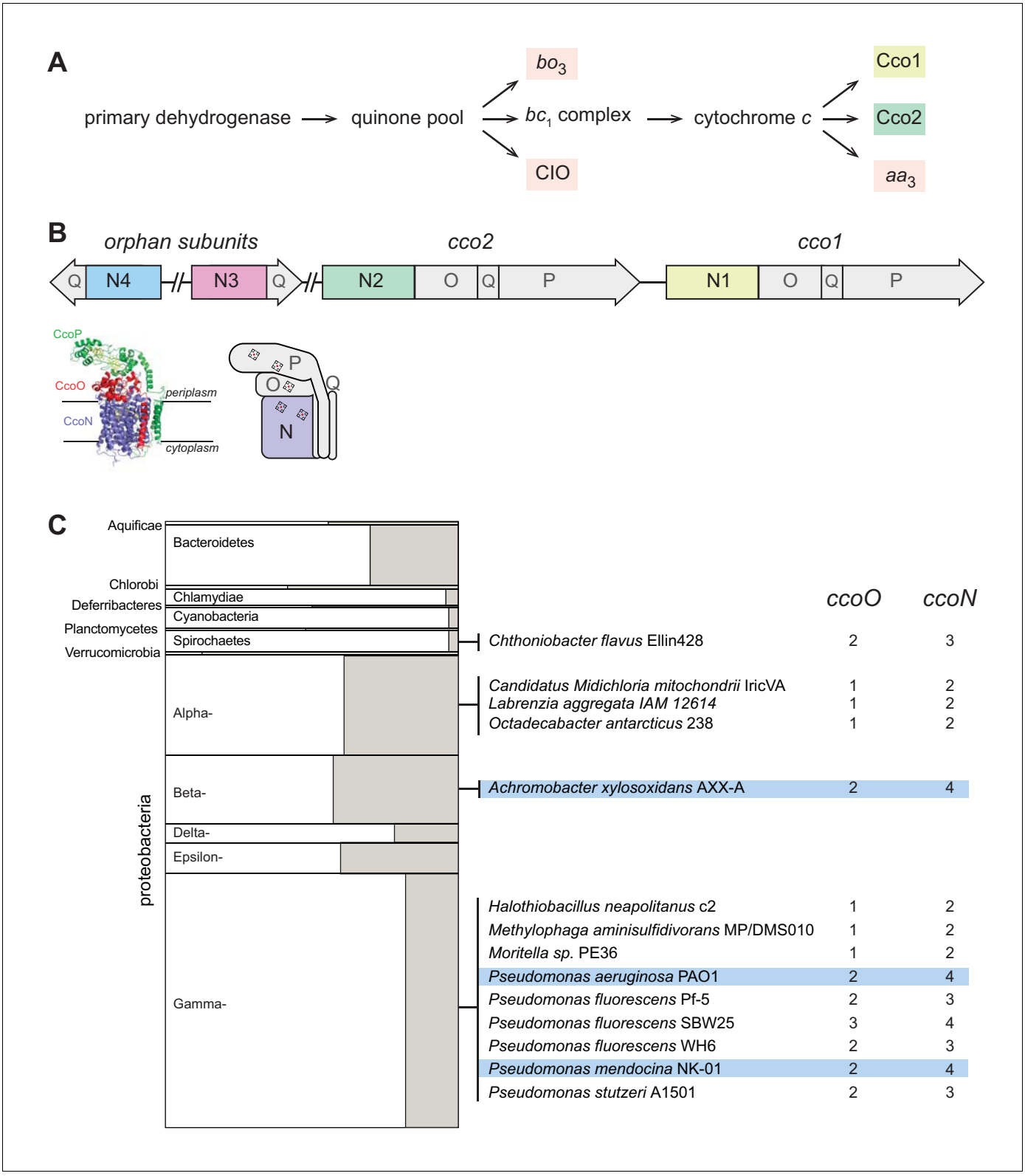

Figure 1. The respiratory chain and arrangement of *cco* genes and protein products in *P. aeruginosa*, and the phylogenetic distribution of orphan *ccoN* genes. (**A**) Branched electron transport chain in *P. aeruginosa*, containing five canonical terminal oxidases. (**B**) Organization of *cco* genes in the *P. aeruginosa* genome. The cartoon of the Cco complex is based on the Cco structure from *P. stutzeri* (PDB: 3mk7) (***Buschmann et al., 2010***). (**C**) Left: graphical representation of the portion of genomes in each bacterial phylum that contain *ccoO* and *N* homologs. The clades Chrysiogenetes,

Figure 1 continued on next page

Figure 1 continued

Gemmatimonadetes, and Zetaproteobacteria were omitted because they each contain only one species with *ccoO* and *N* homologs. The height of each rectangle indicates the total number of genomes included in the analysis. The width of each shaded rectangle represents the portion of genomes that contain *ccoN* homologs. Middle: genomes that contain more *ccoN* than *ccoO* homologs (indicating the presence of orphan *ccoN* genes) are listed. Right: numbers of *ccoO* and *ccoN* homologs in each genome. Blue highlights genomes containing more than one orphan *ccoN* homolog.
DOI: https://doi.org/10.7554/eLife.30205.003

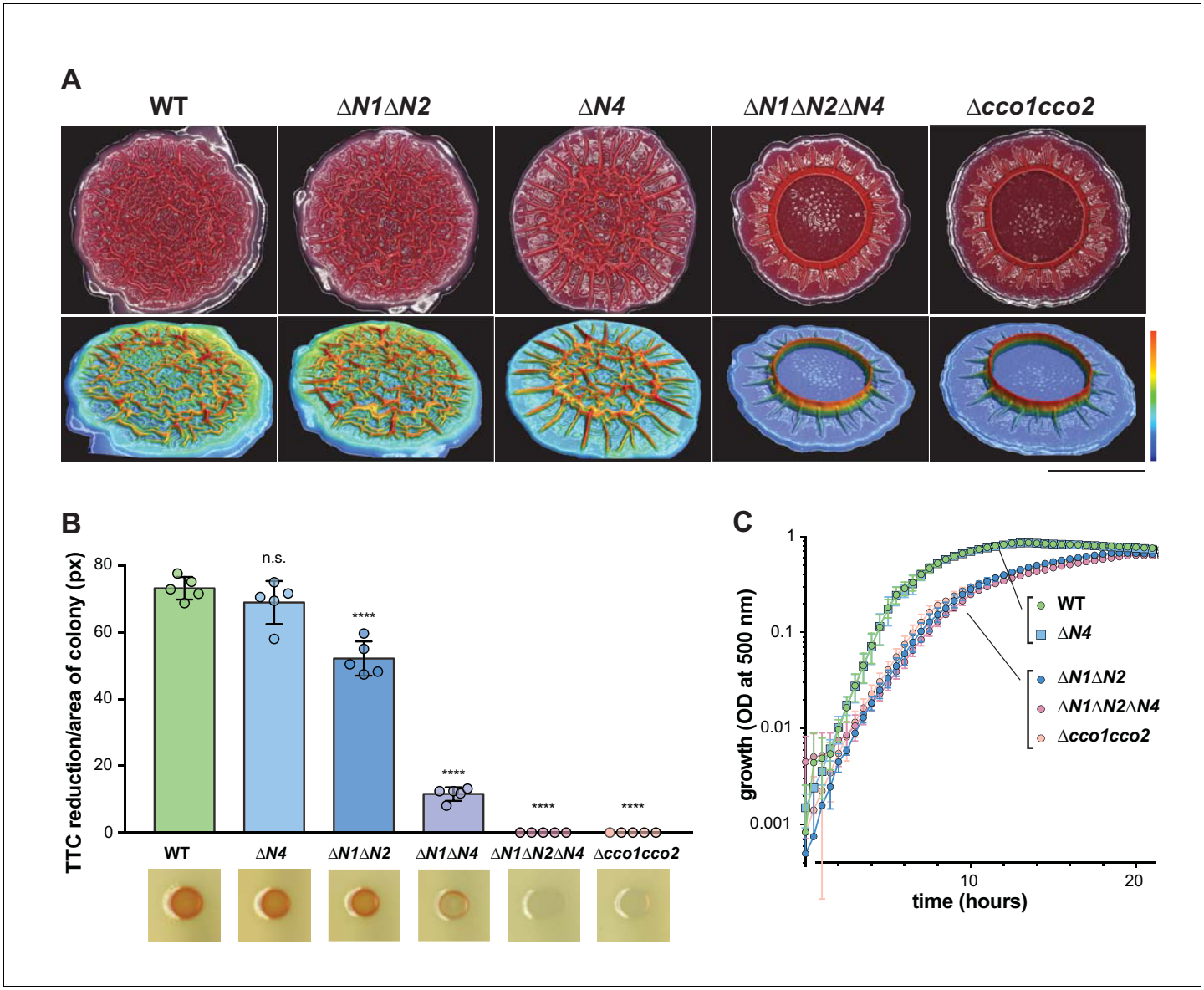

Figure 2. CcoN4-containing heterocomplexes make biofilm-specific contributions to morphogenesis and respiration. (**A**) Top: Five-day-old colony biofilms of PA14 WT and *cco* mutant strains. Biofilm morphologies are representative of more than 10 biological replicates. Images were generated using a digital microscope. Scale bar is 1 cm. Bottom: 3D surface images of the biofilms shown in the top panel. Images were generated using a wide-area 3D measurement system. Height scale bar: bottom (blue) to top (red) is 0–0.7 mm for WT, Δ*N1*Δ*N2*, and Δ*N4*; 0–1.5 mm for Δ*N1*Δ*N2*Δ*N4* and Δ*cco1cco2*. (**B**) TTC reduction by WT and *cco* mutant colonies after 1 day of growth. Upon reduction, TTC undergoes an irreversible color change from colorless to red. Bars represent the average, and error bars represent the standard deviation, of individually-plotted biological replicates (n = 5). p-Values were calculated using unpaired, two-tailed t tests comparing each mutant to WT (****$p \leq 0.0001$). (**C**) Mean growth of PA14 WT and *cco* mutant strains in MOPS defined medium with 20 mM succinate. Error bars represent the standard deviation of biological triplicates.

DOI: https://doi.org/10.7554/eLife.30205.004

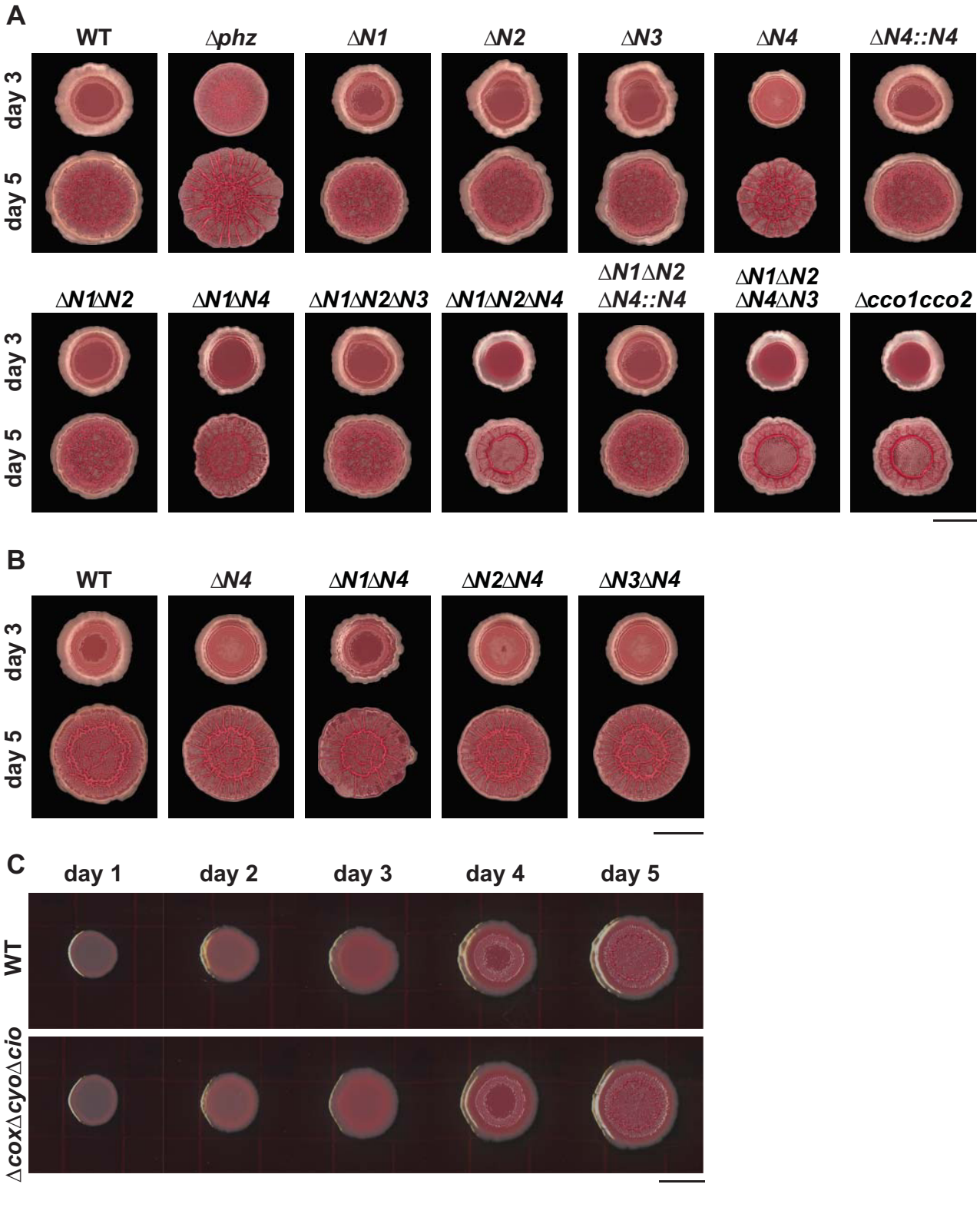

Figure 2—figure supplement 1. Effects of individual and combined *cco* gene deletions on colony biofilm morphogenesis. (**A**) Morphologies of WT, Δ*phz*, and *cco* single, combinatorial, and *ccoN4* complementation strains after 3 and 5 days of incubation. Images shown are representative of at least 5

Figure 2—figure supplement 1 continued on next page

Figure 2—figure supplement 1 continued

biological replicates and were generated using a digital microscope. Scale bar is 1 cm. (**B**) Development of WT, Δ*N4* and N subunit double mutants containing Δ*N4*. Images shown are representative of at least 3 biological replicates and were generated using a digital microscope. Scale bar is 1 cm. (**C**) Development of WT and the triple mutant Δ*cox*Δ*cyo*Δ*cio* in which only the cbb_3-type terminal oxidases are present. Images were generated using a flatbed scanner and are representative of at least 3 biological replicates. Scale bar is 1 cm.

DOI: https://doi.org/10.7554/eLife.30205.005

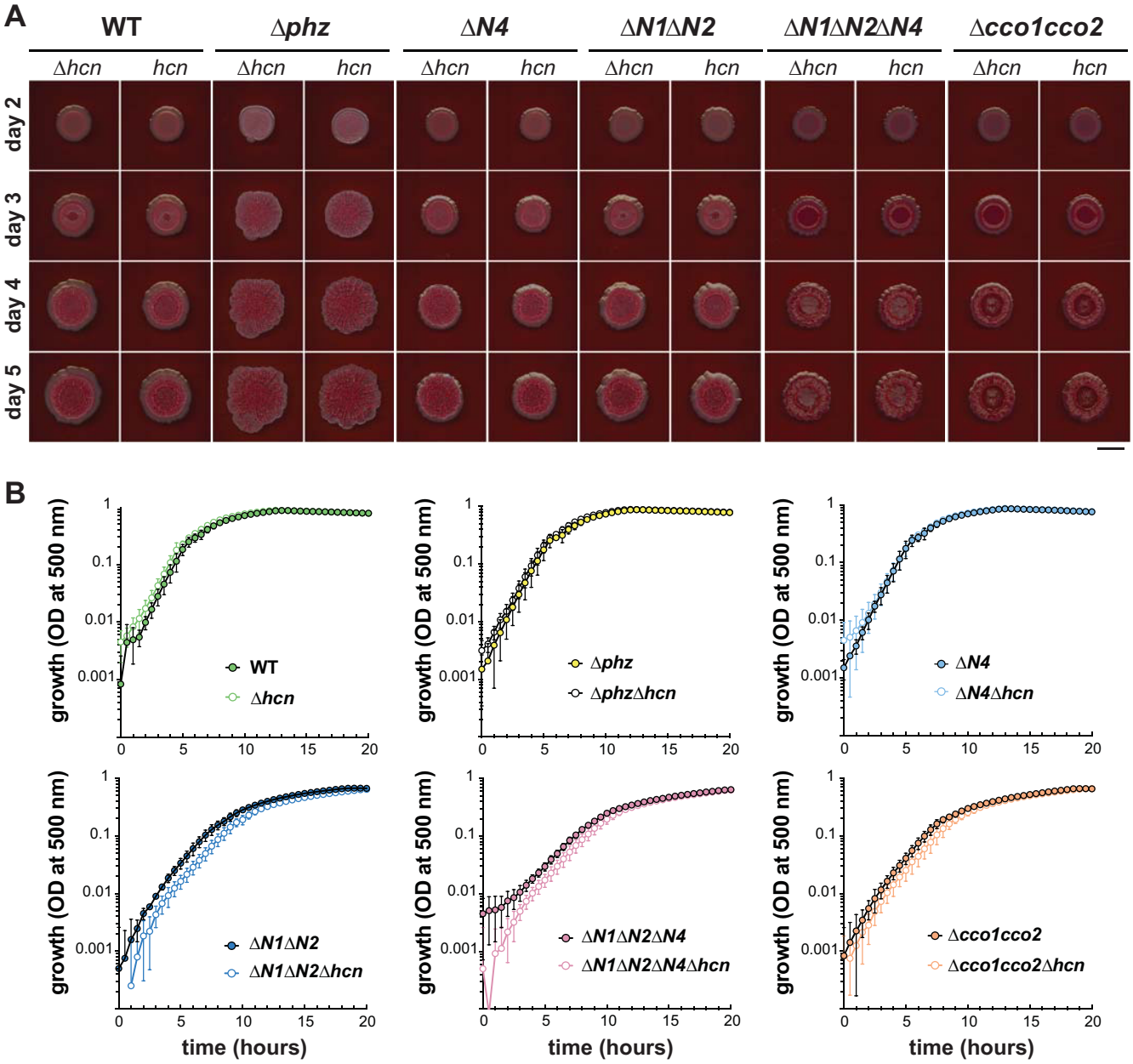

Figure 2—figure supplement 2. PA14 WT, Δ*phz*, and *cco* mutant growth phenotypes are unaffected by endogenous cyanide production. (**A**) Colony development over 4 days for Δ*phz*, Δ*hcnABC*, and *cco* combinatorial mutants. Images were generated using a flatbed scanner and are representative of at least 3 biological replicates. Scale bar is 1 cm. (**B**) Growth of Δ*phz*, Δ*hcnABC*, and *cco* combinatorial mutants in MOPS defined medium with 20 mM succinate. Error bars represent the standard deviation of biological triplicates and are not shown in cases where they would be obscured by the point marker.

DOI: https://doi.org/10.7554/eLife.30205.006

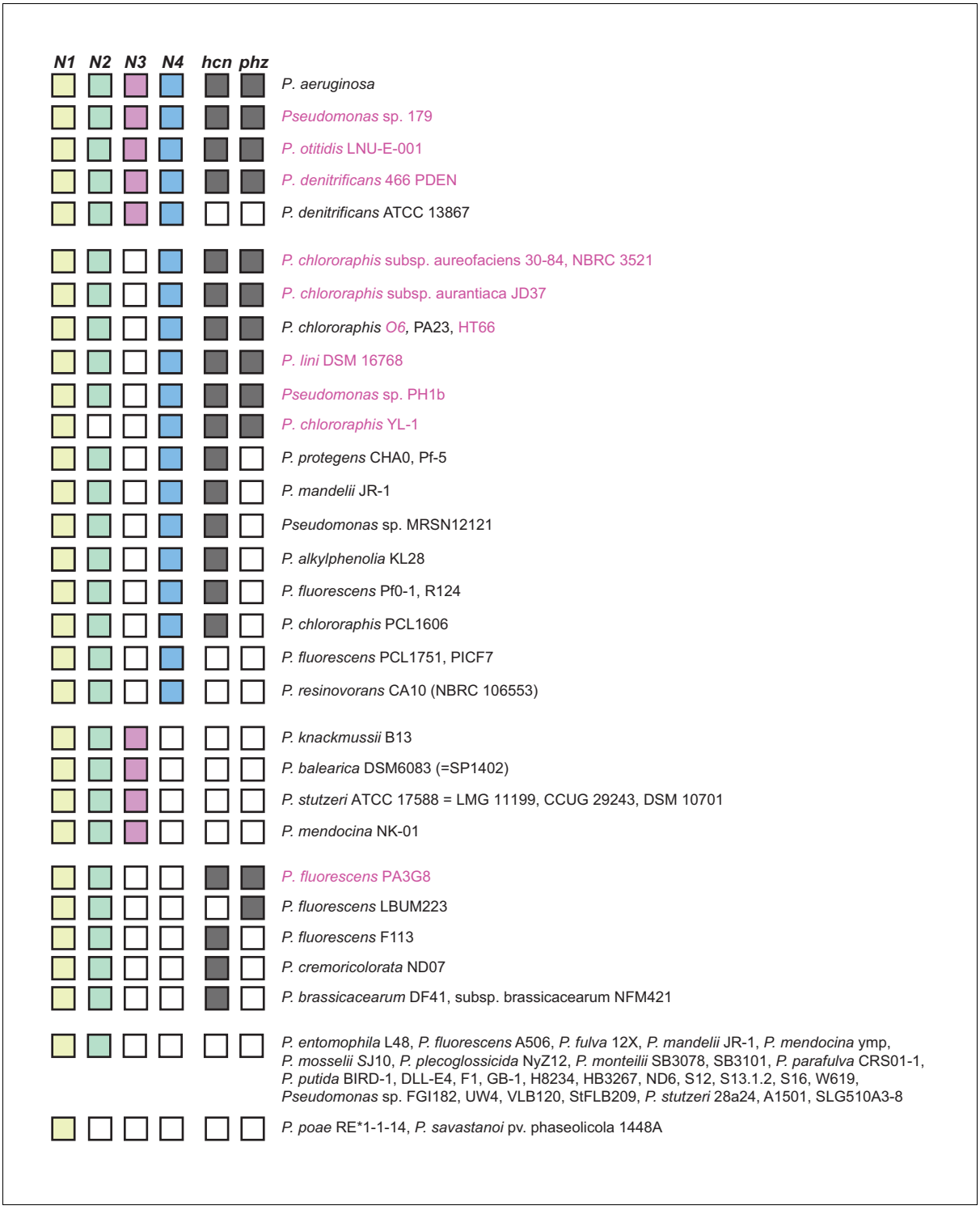

Figure 2—figure supplement 3. Pseudomonads with CcoN homologs. We examined genomes available in the Pseudomonas Genome Database (***Winsor et al., 2016***) for CcoN homologs by performing a protein BLAST search on CcoN1 from *P. aeruginosa* PA14. All hits from full genomes, excluding other *P. aeruginosa* strains, were aligned using ClustalW and a tree was built using the geneious tree builder (Geneious 10 (***Kearse et al., 2012***)). We also included draft genomes that contained genes involved in phenazine biosynthesis (highlighted in purple). The tree revealed four clusters, each being more closely related to one of the four N subunits from PA14, which allowed us to annotate the N subunits accordingly. We next probed all genomes with N subunits for the presence of genes involved in cyanide synthesis (*hcnABC*) and phenazine biosynthesis (*phzABCDEFG*). We did not find a clear correlation between the presence of CcoN4 and Hcn proteins (***Hirai et al., 2016***). We note that with the exception of two *P. fluorescens* strains, those containing *phzABCDEFG* operons also contained *ccoN4*.

DOI: https://doi.org/10.7554/eLife.30205.007

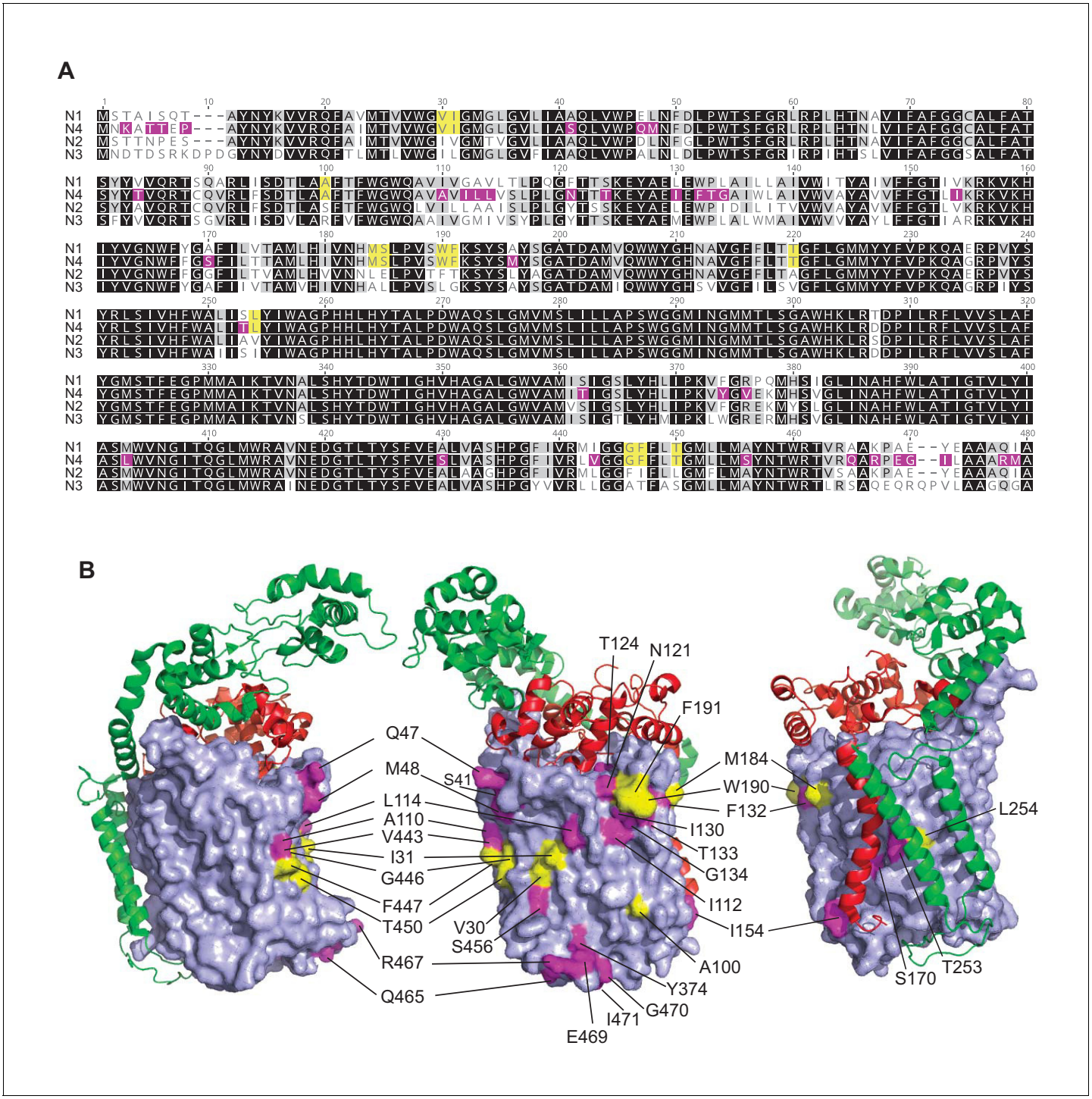

Figure 2—figure supplement 4. Comparison of the PA14 CcoN subunit sequences and analysis of the predicted structure of CcoN4. (**A**) Amino acid alignment (ClustalW) of the four CcoN subunits encoded by the PA14 genome. Residues conserved among all four N subunits are highlighted in black; residues conserved among any three of the four N subunits in gray; residues shared exclusively between CcoN1 and CcoN4 in yellow; and residues unique to CcoN4 in purple. (**B**) Predicted structure of CcoN4 from *P. aeruginosa* PA14, obtained by threading the PA14 sequence through the reported structure for the CcoN subunit of *P. stutzeri* (PDB: 5DJQ; ***Buschmann et al., 2010***) using SWISS-MODELL (***Biasini et al., 2014***). Surface-exposed residues that are shared exclusively between CcoN1 and CcoN4 are shown in yellow, while residues that are unique to CcoN4 are shown in magenta. Ribbon structures of the CcoO and CcoP subunits from *P. stutzeri* are shown in red and green, respectively. Structures were generated using PyMol (***Schrödinger, LLC, 2015***).

DOI: https://doi.org/10.7554/eLife.30205.008

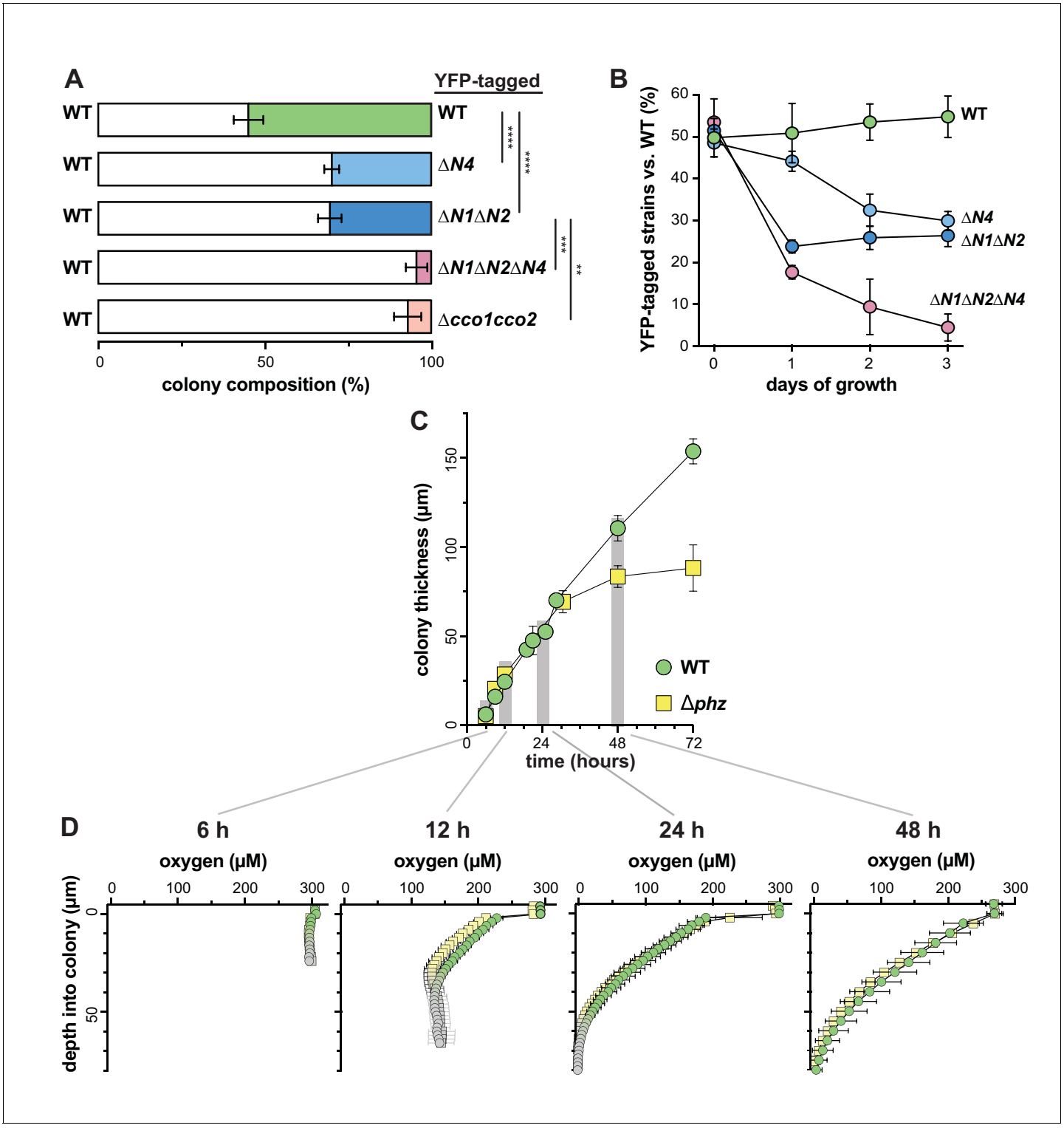

Figure 3. CcoN4 confers a competitive advantage in biofilms, particularly when O_2 becomes limiting. (**A**) Relative fitness of various YFP-labeled *cco* mutants when co-cultured with WT in mixed-strain biofilms for 3 days. Error bars represent the standard deviation of biological triplicates. p-Values were calculated using unpaired, two-tailed t tests (**p≤0.01; ***p≤0.001; ****p≤0.0001). (**B**) Time course showing relative fitness, over a period of 3 days, of various *cco* mutants when co-cultured with WT in mixed-strain biofilms. Results are shown for experiments in which the WT was co-cultured with various 'labeled' strains, that is, those that were engineered to constitutively express YFP. (See ***Figure 3—figure supplement 1*** for results from experiments in which the labeled WT was co-cultured with unlabeled mutants.) Error bars represent the standard deviation of biological triplicates. (**C**) Change in thickness over 3 days of development for colony biofilms of WT and Δ*phz* as assessed by thin sectioning and DIC microscopy. After the

Figure 3 continued on next page

Figure 3 continued

onset of wrinkling, thickness was determined for the base (i.e. the 'valley' between wrinkles). Error bars represent the standard deviation of biological triplicates. (**D**) O_2 profiles of colonies at selected timepoints within the first 3 days of biofilm development. Gray point markers indicate measurements made in the agar directly below the colony. Error bars denote standard deviation of biological triplicates.

DOI: https://doi.org/10.7554/eLife.30205.009

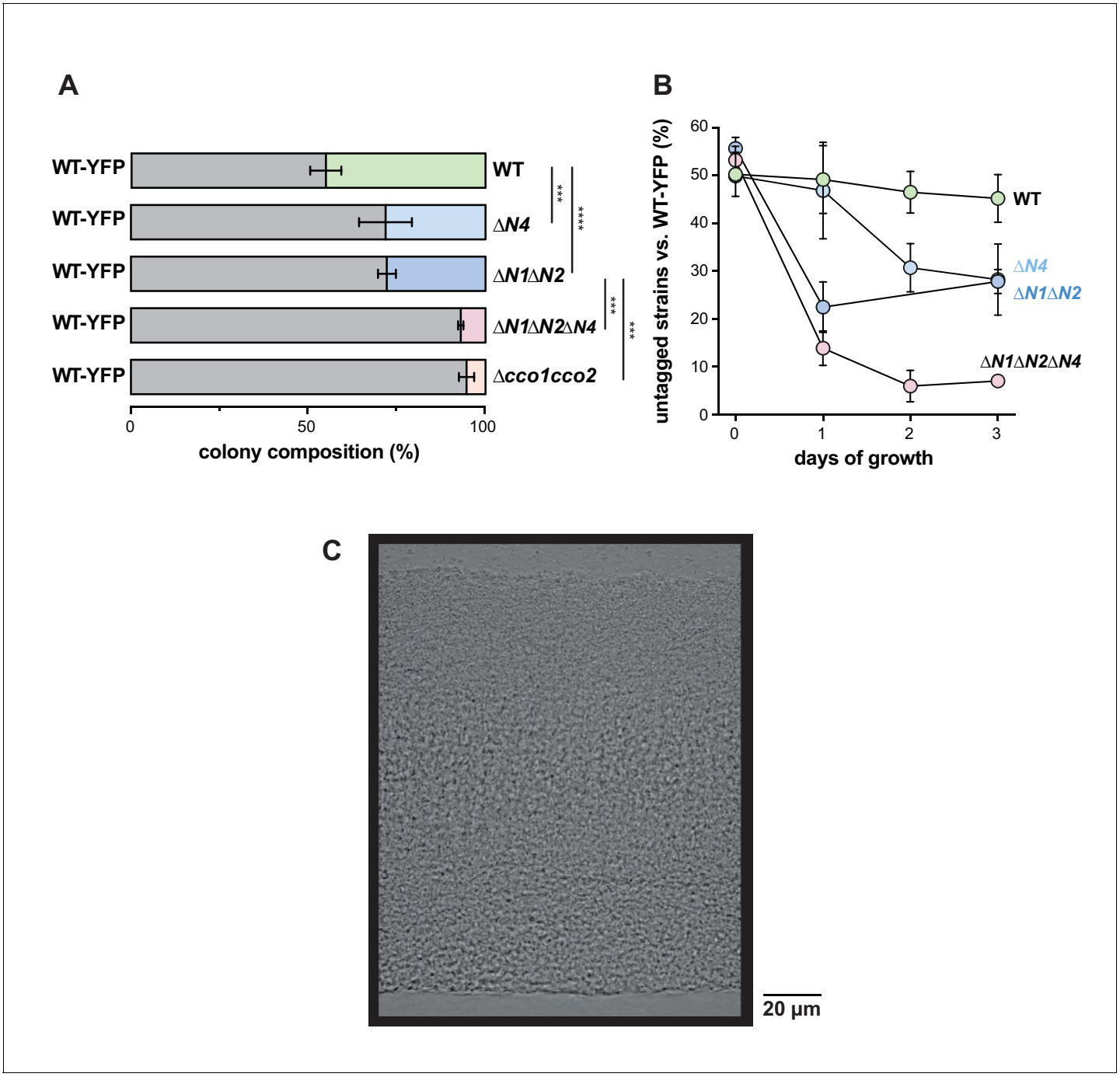

Figure 3—figure supplement 1. CcoN4 is necessary for optimal fitness in biofilms, particularly when O_2 becomes limiting. (**A**) Relative fitness of YFP-labeled WT when co-cultured with various *cco* mutant strains in mixed-strain biofilms for 3 days. Error bars represent the standard deviation of biological triplicates. p-Values were calculated using unpaired, two-tailed t tests (***p≤0.001; ****p≤0.0001). (**B**) Time course showing relative fitness, over a period of 3 days, of YFP-labeled WT when co-cultured with various *cco* mutant strains in mixed-strain biofilms. Error bars represent the standard deviation of biological triplicates. (**C**) DIC image of a 3-day-old WT biofilm, which is representative of at least 10 biological replicates.

DOI: https://doi.org/10.7554/eLife.30205.010

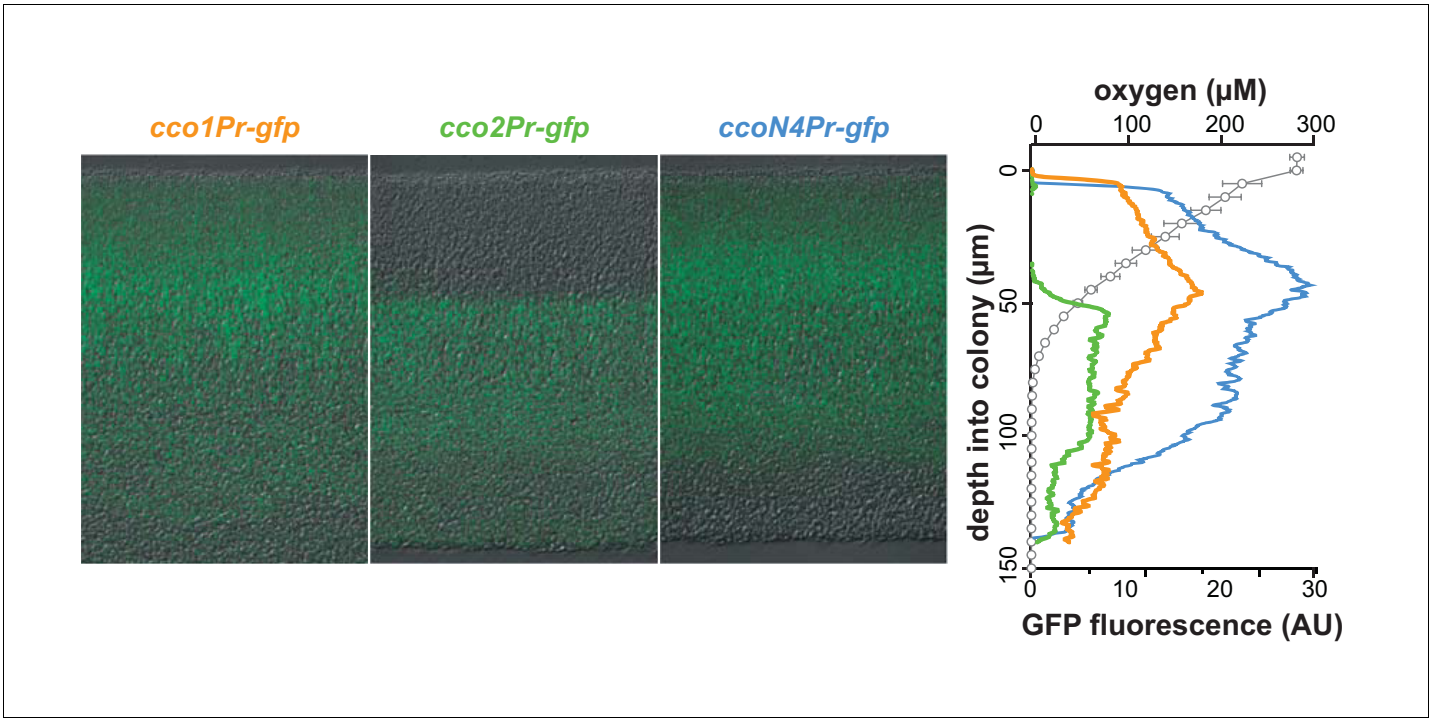

Figure 4. *cco* genes are differentially expressed over biofilm depth. Left: Representative images of thin sections prepared from WT biofilms grown for 3 days. Each biofilm is expressing a translational GFP reporter under the control of the *cco1*, *cco2*, or *ccoN4Q4* promoter. Reporter fluorescence is shown in green and overlain on respective DIC images. Right: Fluorescence values corresponding to images on the left. Fluorescence values for a strain containing the *gfp* gene without a promoter (the empty MCS control) have been subtracted from each respective plot. O_2 concentration over depth (open circles) from 3-day-old WT biofilms is also shown. Error bars represent the standard deviation of biological triplicates and are not shown in cases where they would be obscured by the point markers. y-axis in the right panel provides a scale bar for the left panel. Reporter fluorescence images and values are representative of 4 biological replicates.

DOI: https://doi.org/10.7554/eLife.30205.011

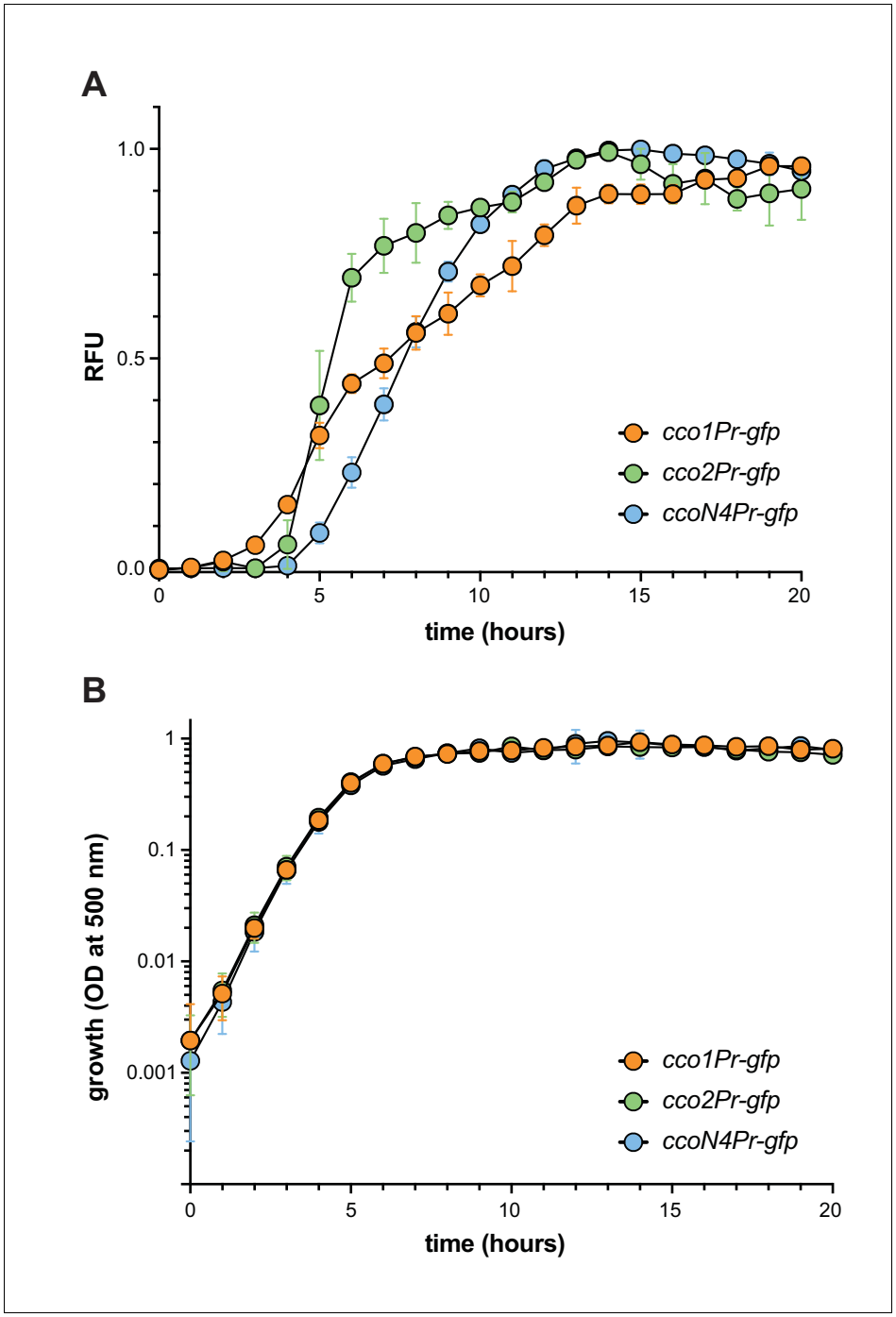

Figure 4—figure supplement 1. Expression of *cco* reporters in shaken liquid cultures. (**A**) Fluorescence of translational reporter strains, engineered to express GFP under the control of the *cco1*, *cco2*, or *ccoN4Q4* promoter during growth in 1% tryptone. Fluorescence values for a strain containing the *gfp* gene without a promoter (the MCS control) were treated as background and subtracted from each growth curve. (**B**) Liquid-culture growth of translational reporter strains in 1% tryptone. Error bars in (**A**) and (**B**) represent the standard deviation of biological triplicates and are not drawn in cases where they would be obscured by point markers.
DOI: https://doi.org/10.7554/eLife.30205.012

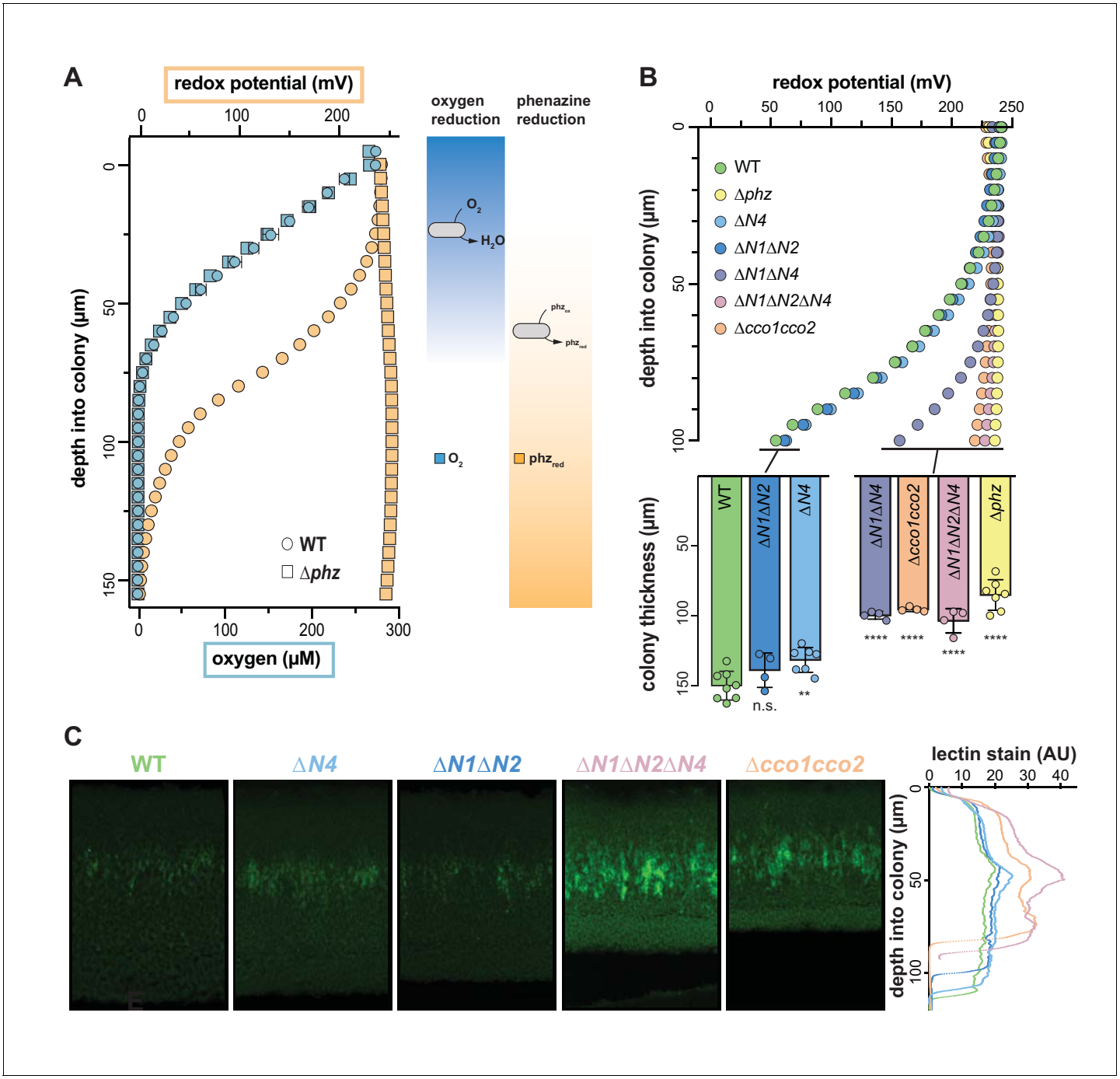

Figure 5. Characterization of chemical gradients and matrix distribution in PA14 WT and mutant colony biofilms. (**A**) Left: Change in O_2 concentration (blue) and redox potential (orange) with depth for WT and Δ*phz* biofilms grown for two days. WT biofilms are ~150 µm thick while Δ*phz* biofilms are ~80 µm thick. For O_2 profiles, error bars represent the standard deviation of biological triplicates. For redox profiles, data are representative of at least 5 biological replicates. Right: model depicting the distribution of O_2 and reduced vs. oxidized phenazines in biofilms. (**B**) Top: Change in redox potential with depth for WT and various mutant biofilms grown for 2 days. Data are representative of at least 5 biological replicates. Bottom: Thickness of 3-day-old colony biofilms of the indicated strains. Bars represent the average of the plotted data points (each point representing a biological replicate, $n \geq 4$), and error bars represent the standard deviation. p-Values were calculated using unpaired, two-tailed t tests comparing each mutant to WT (n.s., not significant; **$p \leq 0.01$; ****$p \leq 0.0001$). (**C**) Left: Representative thin sections of WT and *cco* mutant biofilms, stained with lectin and imaged by fluorescence microscopy. Biofilms were grown for 2 days before sampling. Right: Relative quantification of lectin stain signal intensity. Coloration of strain names in the left panel provides a key for the plotted data, and the y-axis in the right panel provides a scale bar for the left panel. Lectin-staining images and values are representative of 4 biological replicates.

DOI: https://doi.org/10.7554/eLife.30205.013

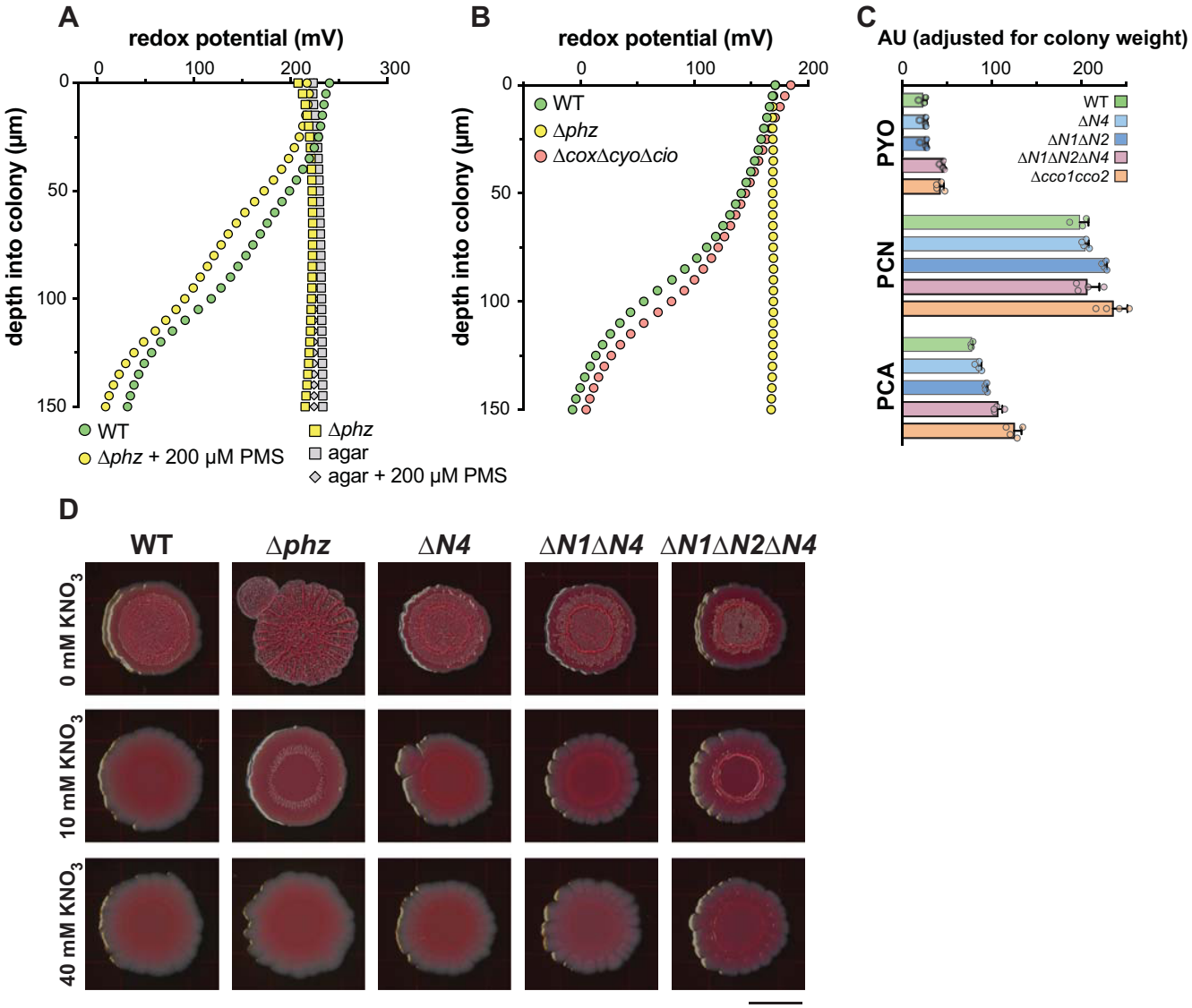

Figure 5—figure supplement 1. Use of a redox microelectrode to measure phenazine reduction in colony biofilms. (**A**) Change in redox potential over depth for 2-day-old biofilms of PA14 WT, Δ*phz*, and Δ*phz* grown on 200 µM phenazine methosulfate (PMS). Data are representative of at least 3 biological replicates. To ensure that addition of PMS did not alter the baseline redox potential, a measurement was also taken of agar only. (**B**) Change in redox potential with depth for WT, Δ*phz*, and Δ*cox*Δ*cyo*Δ*cio* biofilms grown for 2 days. Data are representative of at least 2 biological replicates. (**C**) Levels of phenazines extracted from the agar medium underneath the colony and separated by HPLC, adjusted for biomass, for PA14 WT and various *cco* mutant biofilms grown for 2 days. Data represent the area under each peak in absorbance units for the phenazines indicated, and error bars represent standard deviation of at least 3 biological replicates. The phenazines pyocyanin (PYO), phenazine-1-carboxamide (PCN), and phenazine-1-carboxylic acid (PCA) were quantified. (**D**) Colony biofilm morphologies on day 4 of development for WT and various *cco* mutant biofilms grown on colony morphology plates containing 0, 10, and 40 mM potassium nitrate. Images were generated using a flatbed scanner and are representative of at least 3 biological replicates. Scale bar is 1 cm.

DOI: https://doi.org/10.7554/eLife.30205.014

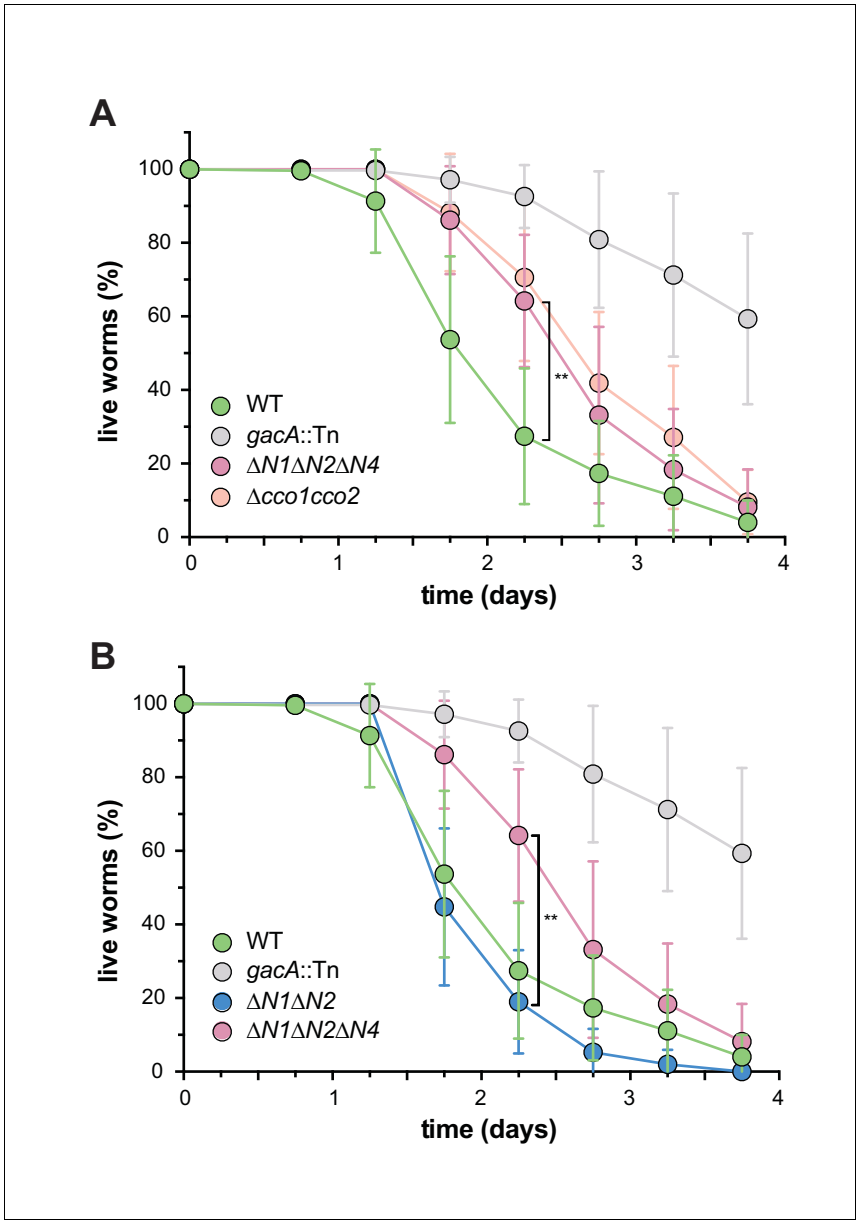

Figure 6. CcoN4-containing isoform(s) make unique contributions to PA14 virulence. Slow-killing kinetics of WT, *gacA*, and various *cco* mutant strains in the nematode *Caenorhabditis elegans*. Nearly 100% of the *C. elegans* population exposed to WT PA14 is killed after 4 days of exposure to the bacterium, while a mutant lacking GacA, a regulator that controls expression of virulence genes in *P. aeruginosa*, shows decreased killing, with ~50% of worms alive 4 days post-exposure. (**A**) Δ*N1*Δ*N2*Δ*N4* and Δ*cco1cco2* show comparably attenuated pathogenicity relative to WT. Error bars represent the standard deviation of at least 6 biological replicates. At 2.25 days post-exposure, significantly less *C. elegans* were killed by Δ*N1*Δ*N2*Δ*N4* than by WT (unpaired two-tailed t test; p=0.0022). (**B**) Δ*N1*Δ*N2* displays only slightly reduced pathogenicity when compared to WT. At 2.25 days post-exposure, significantly more *C. elegans* were killed by Δ*N1*Δ*N2* than by Δ*N1*Δ*N2*Δ*N4* (unpaired two-tailed t test; p=0.003). Error bars represent the standard deviation of at least 4 biological replicates, each with a starting sample size of 30–35 worms per replicate.

DOI: https://doi.org/10.7554/eLife.30205.015